Robust Covariance Matrix Estimation with Application to Volcano Monitoring using SAR Image Stacks

Yuanyuan, Wang, Technische Universität München, wang@bv.tum.de, Germany
Xiao Xiang, Zhu, German Aerospace Center & Technische Universität München, xiao.zhu@dlr.de, Germany
Richard, Bamler, German Aerospace Center & Technische Universität München, Germany

Abstract

This paper introduces a new method – the *Rank M-Estimator* (RME) – for robust covariance matrix estimation of distributed scatterers (DSs) in SAR image stacks, or more general for complex multivariate with multiplicative and non-stationay phase signal. The RME can work without the assumption of samples' stationarity, which is seldom addressed in the SAR community. In other words, no flattening/estimation of the interferometric phase is required. The robustness of RME is achieved by using an M-estimator, i.e. amplitude-based weighing function in covariance estimation.

1 Introduction

Monitoring volcanic regions using InSAR methods encounters multiple challenges: 1. limited number of persistent scatterer (PS), 2. low number of images, and 3. sometimes the precipitous topography causes height dependent tropospheric delay (TD) which correlates the deformation signal.

To cope with the low PS density, distributed scatterers (DSs) are usually exploited, such as algorithms like SqueeSAR [1] and so on [2]–[4]. They perform a statistical test on the amplitude of the neighbourhood of a target pixel, in order to identify its "brother pixels" realized from the same distribution. The mean of these brother pixels is then taken, and treated as a PS in the subsequent processing. Slightly different in [2], the phase history parameters of each single-look DS pixel is retrieved by the optimal maximum likelihood estimator (MLE) assuming complex circular Gaussian (CCG) distributed DS.

Nevertheless, all the aforementioned algorithms rely on the statistical test on the amplitude time series of the neighbouring pixels. The detection rate (different distribution detected as different distribution) of the test degrades with decreasing number of images. According to [5], under the assumption of Rayleigh distributed amplitude time series, the detection rate (at constant 5% false alarm rate) is only 20% using 10 images for two DSs with an expected intensity ratio of 3 dB using the *Kolmogorov-Smirnov* (KS) test employed in SqueeSAR. As the detection rate goes down, pixels of different distributions including non-Gaussian ones are included in the covariance matrix estimation. This in turn affects the final parameter estimation.

The purpose of this paper is to introduce a robust and adaptive covariance matrix estimator when the selected neighbourhood is contaminated. We consider two types of contamination: 1. non-Gaussian samples, and 2. non-stationary (N-S) samples. For the first type, an M-estimator with amplitude-based weighting is employed, and for the second type we use higher order moments to cancel the effect of multiplicative mean. The combination of these two aspects leads to our proposal of the *Rank M-Estimator* (RME).

2 Robust covariance matrix estimation

2.1 MLE under complex circular Gaussian distribution

The covariance of two single-look complex observations g_n and g_k in image n and k is defined as the expectation of the product of one with the complex conjugate of the other: $c_{n,k} = E\left(g_n g_k^*\right)$. The MLE of the covariance matrix of N-variate CCG vector $\mathbf{g}$ is:

$$\hat{\mathbf{C}}_{MLE} = \frac{1}{M}\sum_{m=1}^{M}\mathbf{g}(m)\mathbf{g}(m)^H \tag{1}$$

where $\mathbf{g}(m)$ is $\left[g_1(m) \;\; g_2(m) \;\; \cdots \;\; g_N(m)\right]^T$, and the M samples are assumed to be spatially stationary.

2.2 M-estimator of covariance

The M-estimator is a generalization of the MLE that can be designed to, e.g., resist outliers [6]. It minimizes a customized loss function $\rho(x)$ w.r.t. the residual x. The M-estimator of a covariance matrix is [7]:

$$\hat{\mathbf{C}}_{M-est} = \arg\min_{\mathbf{C}}\sum_{m=1}^{M}\rho\left(x\left(\mathbf{C},m\right)\right) \tag{2}$$

where $x^2\left(\mathbf{C},m\right) = \mathbf{g}(m)^H\mathbf{C}^{-1}\mathbf{g}(m)$. This can be solved in general by an iteratively reweighted approach [8]:

$$\hat{\mathbf{C}}_{k+1} = \frac{1}{M}\sum_{m=1}^{M}w\left(x\left(\hat{\mathbf{C}}_k,m\right)\right)\mathbf{g}(m)\mathbf{g}(m)^H \tag{3}$$

where the real-valued weighting function $w(x)$ is $\rho'(x)/x$.

The MLE of CCG multivariate corresponds to an M-estimator with a loss function $\rho(x)=x^2$, i.e.:

$$\hat{\mathbf{C}}_{MLE}=\arg\min_{\mathbf{C}}\sum_{m=1}^{M}\mathbf{g}(m)^H\mathbf{C}^{-1}\mathbf{g}(m).$$

It is evident, for CCG MLE, a single outlier in the samples will steer the estimator towards the outlier, and can considerably bias the estimation. However, the M-estimator down-weights the highly deviating samples according to the weighting function.

In application to SAR image, instead of CCG, one can model a time series of pixel as complex circular t-distribution (CCT) with a degree of freedom ν. The CCT approaches CCG as ν approaches $+\infty$, and become more heavily tailed as ν approaches 0. [9] used the weighting function $w(x)=(2N+\nu)/(\nu+2x^2)$, which corresponds to the MLE of the covariance under CCT.

Unfortunately, the sample distribution is always varying and unknown, i.e. ν is unknown. In addition, with real data when the number of images is low, mixture of distributions among samples can occur even with the adaptive sample selection. Therefore, without knowledge of the sample distribution, one can assume ν approaches 0, and the multivariate **g** is i.i.d., i.e. $\mathbf{C}=\overline{I}\,\mathbf{I}$ where $\overline{I}$ is the expected intensity and **I** is the identity matrix. This literally assumes the samples are very heavily tailed, and contain no correlation between different images. It leads to an interesting weighting function:

$$w=\frac{N\overline{I}}{\|\mathbf{g}(m)\|^2} \tag{4}$$

which is the ratio of the expected intensity in space (assumed constant) and time (depends on sample). Finally, the covariance matrix estimate is:

$$\hat{\mathbf{C}}_{SCM}=\frac{N\overline{I}}{M}\sum_{m=1}^{M}\|\mathbf{g}(m)\|^{-2}\mathbf{g}(m)\mathbf{g}(m)^H. \tag{5}$$

This specific M-estimator is also known as the *sign* covariance matrix (SCM) [10], where only the "sign" or "direction" of **g** is considered. Therefore, the real covariance is lost, yet the shape and orientation of the joint distribution of **g** is preserved. If the exact covariance shall be retrieved, one could always estimate it from the eigenvectors of $\hat{\mathbf{C}}_{SCM}$ and the samples. Experiment found $\hat{\mathbf{C}}_{SCM}$ is very stable for TerraSAR-X (TS-X) high resolution spotlight data.

2.3 The Rank M-estimator for non-stationary samples

So far, all the aforementioned estimators are all based on spatially stationary samples, i.e. identical expected interferometric phase. For N-S samples, it is a joint estimation of the expected interferometric phase and the covariance [11], i.e.:

$$\hat{\mathbf{C}}_{MLE}=\frac{1}{M}\sum_{m=1}^{M}\hat{\mathbf{\Phi}}(m)^H\mathbf{g}(m)\mathbf{g}(m)^H\hat{\mathbf{\Phi}}(m) \tag{6}$$

where $\hat{\mathbf{\Phi}}(m)$ is the diagonal matrix containing the estimated phase values of $\mathbf{g}(m)$.

The estimation of interferometric phase is usually done by spatial filtering. The performance greatly depends on the filter itself. And it can be challenging in urban area. In [2], it is dealt by a multi-resolution defringe algorithm. Nevertheless, the phase estimation requires additional effort and bad estimates largely affect the covariance matrix estimation.

Therefore, we need an estimator that is invariant of the multiplicative phase signal. Inspired by the rank covariance matrix (RCM) for additive noise explained in [10], we introduce the RCM for complex multivariate with multiplicative phase signal, which is:

$$\hat{\mathbf{C}}_{RCM}=\frac{1}{M}\sum_{m=1}^{M}\hat{\mathbf{r}}(m)\hat{\mathbf{r}}(m)^H, \tag{7}$$

$$\text{where } \hat{\mathbf{r}}(m)=\frac{1}{J}\sum_{j=1}^{J}\mathbf{g}(m)\bullet\mathbf{g}(j)^* \quad m\neq j \tag{8}$$

can be regarded as the *rank* vector of **g** in multiplicative. $\mathbf{g}(j)$ is the neighbourhood of $\mathbf{g}(m)$, and the $\bullet$ denotes the element-wise product. RCM is a fourth order descriptor of **g**, where the multiplicative mean has disappeared due to the complex conjugate. And it can be proven under CCG that $\text{abs}(\hat{\mathbf{C}}_{RCM})$ approaches $\text{abs}(\hat{\mathbf{C}})^{\bullet 2}$ asymptotically, where $^{\bullet 2}$ is the element-wise square.

Based on this, we define the *Rank M-Estimator* with weighting function $w(x)$ analogous to Equation (3):

$$\hat{\mathbf{C}}_{RME,k+1}=\frac{1}{M}\sum_{m=1}^{M}w\left(x\left(\hat{\mathbf{C}}_{RME,k},m\right)\right)\hat{\mathbf{r}}(m)\hat{\mathbf{r}}(m)^H \tag{9}$$

3 Experiments

3.1 Simulations

In this section, the MLE for CCG, the M-Estimator, and the RME are compared under three different scenarios: 1. multivariate CCG, 2. multivariate CCT with degree of freedom 1, and 3. N-S multivariate CCT, i.e. samples contain phase fringes.

For each scenario, the same predefined exponentially delaying coherence matrix is used for DS samples simulation. We simulated ten acquisitions, with each acquisition having 500 samples. In the last scenario, ten constant fringe frequencies within [0 π/100] are randomly picked for the ten acquisitions, respectively.

The results comparison are shown in Figure 1. Each row represents one of the aforementioned three scenarios, and each column represents one of the three covariance

estimators. Subplot (1, 1) shall be regarded as the reference coherence matrix, because the MLE is the optimal estimator under CCG, and asymptotically unbiased when the number of samples are large.

All the three estimators are successful under CCG, except the minor fluctuation of RME at very low coherence due to the square root operation. The MLE fails when the samples are contaminated by outliers, e.g. heavily tailed t-distribution. Yet the M-estimator and RME remain a correct estimation. However, the M-estimator is not capable of dealing with N-S samples. Heavy underestimation occurs. The RME is mean invariant, and keeps good performance at all conditions.

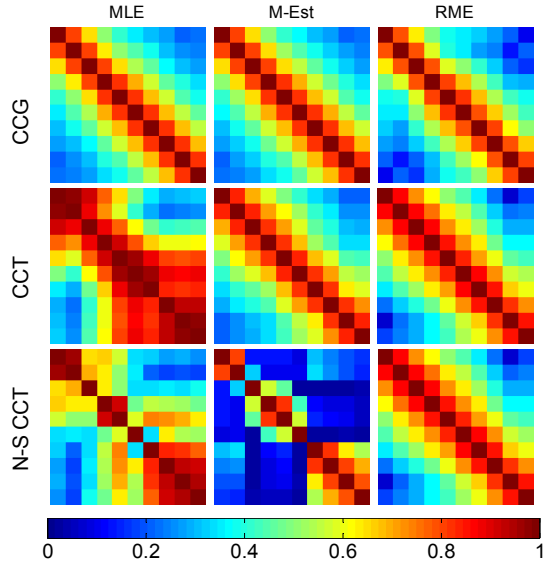

Figure 1. Comparison of covariance matrix estimation using 1st column: MLE (under Gaussian), 2nd column: M-estimator (amplitude-based weighting), and 3rd column: rank M-estimator; under three different cases: 1st row: complex circular Gaussian, 2nd row: complex circular t-distribution with degree of freedom 1, and 3rd column: non-stationary complex circular t-distribution.

3.2 Real data

Two test sites are selected in the super volcano region Campi Flegrei in Italy. We compare the linear deformation rate of the two areas estimated using $\hat{\mathbf{C}}_{MLE}$ and $\hat{\mathbf{C}}_{RME}$, respectively. The DS pixel's deformation rate is estimated using:

$$\{\hat{s},\hat{v}\} = \arg\min_{s,v}\left\{\mathbf{g}^H\boldsymbol{\Phi}(s,v)\hat{\mathbf{C}}^{-1}\boldsymbol{\Phi}(s,v)^H\mathbf{g}\right\} \qquad (10)$$

where s and v are the elevation and linear deformation rate, $\boldsymbol{\Phi}(s,v)$ is the diagonal matrix containing the modelled phase, and $\hat{\mathbf{C}}$ is the covariance matrix (either $\hat{\mathbf{C}}_{MLE}$ or $\hat{\mathbf{C}}_{RME}$). More details can be found in [2]. For each DS pixel, we perform once the adaptively sample selection using the KS test with *ten* TS-X high resolution spotlight images. And the same samples are used for estimating both covariance matrices.

The comparison is plotted in Figure 2, where the upper row corresponds to the results of the first test area, and the second row is the second area. Images on the left column are the results using $\hat{\mathbf{C}}_{MLE}$, and right ones are from $\hat{\mathbf{C}}_{RME}$. The coloured deformation rates w.r.t. a local reference point are overlaid on the SAR intensity image. Since the spans of both two areas are around a few hundreds of meters, homogeneous deformation rates are expected. The first test area contains some buildings and vegetation. And thus, their stationarity is not guaranteed. Therefore, many bad estimates appears like salt and pepper noise if using the conventional $\hat{\mathbf{C}}_{MLE}$. The second area is mostly vegetation, except in the center a road which usually appears as DS in X-band images. The $\hat{\mathbf{C}}_{RME}$ also in general outperforms $\hat{\mathbf{C}}_{MLE}$.

For quantitative comparison, the histograms of the deformation rates enclosed in the two dashed red rectangles in Figure 2 are plotted in the corresponding positions in Figure 3. When using $\hat{\mathbf{C}}_{MLE}$, many local peaks of deformation rate almost uniformly appear in the search range. These peaks should not correspond to deformation signal, except extremely conditions. While using $\hat{\mathbf{C}}_{RME}$, the result is much more homogenous, and thus, more reasonable.

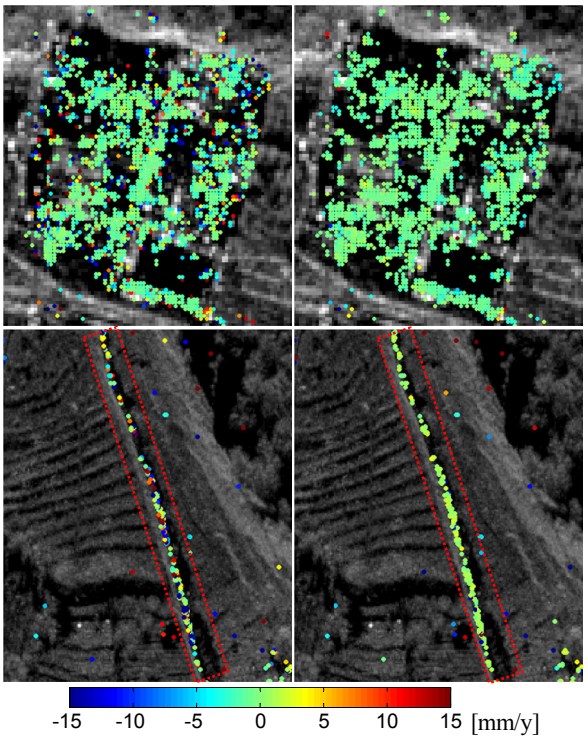

Figure 2. Comparison of deformation rate estimates (overlaid on SAR intensity images) w.r.t. a local reference point of two test areas in the super volcano region Campi Flegrei. Homogenous deformation rate is expected due to the small size of the two areas. The left column is the results using $\hat{\mathbf{C}}_{MLE}$, and the right column is using the robust $\hat{\mathbf{C}}_{RME}$. The samples are identical for both covariance matrices estimation, and they are adaptively selected (KS test) using *ten* images.

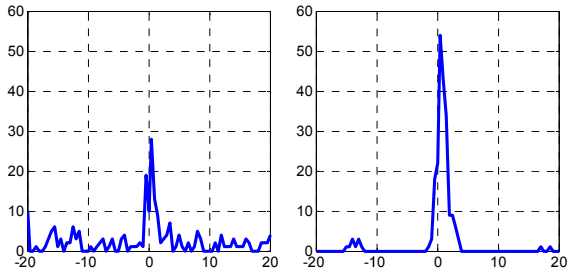

Figure 3. Corresponding histograms of the deformation rates [mm/y] enclosed in the two dashed red rectangles in . Left: result from $\hat{\mathbf{C}}_{MLE}$; and right: result from $\hat{\mathbf{C}}_{RME}$. For the left figure, many local peaks almost uniformly appear in the search range. Most of them should not correspond to deformation signals. While using $\hat{\mathbf{C}}_{RME}$, the result is much more homogenous, and thus, more reasonable.

The proposed algorithm has been integrated into the DLR'S *PSI-GENESIS* system. It is applied on the whole area of the image stack of volcano Campi Flegrei. The stack contains 34 TS-X high resolution spotlight images, spanning from Dec. 2009 to Mar. 2012. The result of using only the PS is shown as the upper plot of Figure 4. The lower one is the result using the proposed RME on DS, combined with the PS result. It retrieves 15 times more scatterers than using the PS only. For good visualization, only 10% of the points from either method are plotted in Figure 4, and the point size is kept the same for both subplots.

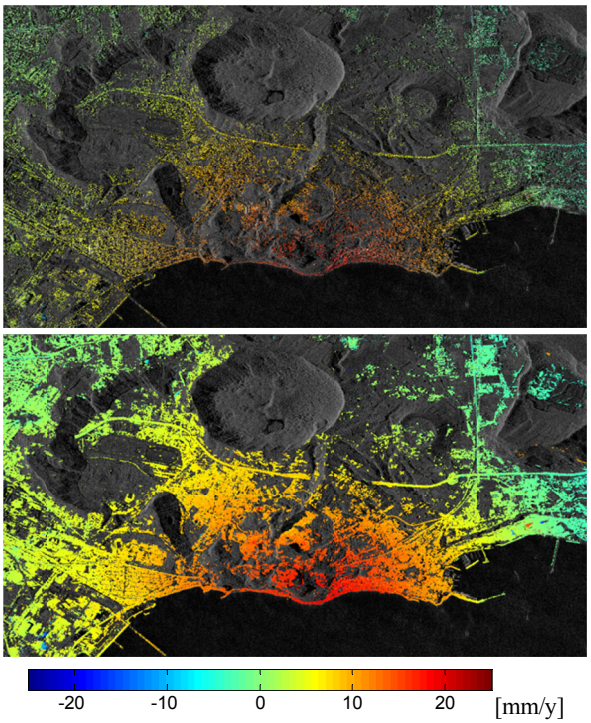

Figure 4. Linear deformation rate of the super volcano Campi Flegrei using only the PS (upper), and using PS+DS with the proposed RME covariance matrix estimation method (lower).

Acknowledgement

This work is partially supported by the Helmholtz Association under the framework of the Young Investigators Group "SiPEO". It is also part of the project "4D City" funded by the IGSSE of TU München and the German Research Foundation (Förderkennzeichen BA2033/3-1). The PS result in the paper is processed by DLR's *PSI-GENESIS* system.

References

[1] A. Ferretti, et al., "A New Algorithm for Processing Interferometric Data-Stacks: SqueeSAR," *IEEE Trans. Geosci. Remote Sens.*, 49(9), 2011.

[2] Y. Wang, et al., "Retrieval of phase history parameters from distributed scatterers in urban areas using very high resolution SAR data," *ISPRS J. Photogramm. Remote Sens.*, vol. 73, Sep. 2012.

[3] K. Goel and N. Adam, "An advanced algorithm for deformation estimation in non-urban areas," *ISPRS J. Photogramm. Remote Sens.*, vol. 73, Sep. 2012.

[4] M. Schmitt and U. Stilla, "Adaptive Multilooking of Airborne Single-Pass Multi-Baseline InSAR Stacks," *IEEE Trans. Geosci. Remote Sens.*, 52(1), 2014.

[5] A. Parizzi and R. Brcic, "Adaptive InSAR Stack Multilooking Exploiting Amplitude Statistics: A Comparison Between Different Techniques and Practical Results," *Geosci. Remote Sens. Lett. IEEE*, 8(3), 2011.

[6] P. J. Huber, *Robust Statistics*. John Wiley & Sons, 1981.

[7] R. A. Maronna, "Robust M-Estimators of Multivariate Location and Scatter," *Ann. Stat.*, 4(1), 1976.

[8] E. Ollila and V. Koivunen, "Influence functions for array covariance matrix estimators," in *Statistical Signal Processing, 2003 IEEE Workshop on*, 2003.

[9] M. Schmitt, et al., "Adaptive Covariance Matrix Estimation for Multi-Baseline InSAR Data Stacks," *IEEE Trans. Geosci. Remote Sens.*, in press, 2014.

[10] S. Visuri, V. Koivunen, and H. Oja, "Sign and rank covariance matrices," *J. Stat. Plan. Inference*, 91(2), pp. 557–575, 2000.

[11] F. De Zan and F. Rocca, "Coherent processing of long series of SAR images," in *Geoscience and Remote Sensing Symposium, 2005. IGARSS '05. Proceedings. 2005 IEEE International*, 2005.